Hierarchical Methodology for the Numerical Simulation of the Flow Field around and in the Wake of Horizontal Axis Wind Turbines: Rotating Reference Frame, Blade Element Method and Actuator Disk Model

by

Teymour Javaherchi, Sylvain Antheaume and Alberto Aliseda

Hierarchical Methodology for the Numerical Simulation of the Flow Field around and in the Wake of Horizontal Axis Wind Turbines: Rotating Reference Frame, Blade Element Method and Actuator Disk Model[*]

Teymour Javaherchi[†1], Sylvain Antheaume[2] and Alberto Aliseda[‡1]
[1]University of Washington, Department of Mechanical Engineering
[2]Institut National Polytechnique de Grenoble

ABSTRACT

A hierarchy of computational methods for Horizontal Axis Wind Turbine (HAWT) flow field is proposed, focusing on rotor models for Reynolds-Averaged Navier-Stokes simulations. Three models are systematically compared to determine their adequacy to capture performance and wake dynamics, and the trade-offs between accuracy and computational cost. The Rotating Reference Frame model is prescribed for detailed flow field studies, specifically at the root and blade tip. The Blade Element Model does not reproduce the near wake region but successfully predicts the velocity deficit in the axisymmetric far wake, and the power and torque coefficients. The Actuator Disk Model underestimates the velocity deficit in the far wake, but can be corrected to perform simulations of large wind farms. This methodology is applied to a canonical rotor and compared against experimental data. These models span three orders of magnitude in computational time and cost for the study of HAWT aerodynamic performance and wake interaction.

1. INTRODUCTION

Computational Fluid Dynamics (CFD) is increasingly used to design and assess new technology in wind energy engineering [1]. Understanding the capabilities and limitations of computational models is therefore an important scientific and technological issue [2], with implications in the economical and efficient development of new generations of turbines, for both the utility and residential markets.

Large scale experimental studies [3, 4, 5] are now available to provide insights into the flow field dynamics and performance of Horizontal Axis Wind Turbines (HAWTs). Computational modeling [6, 7, 8, 9, 10, 11] has taken advantage of these measurements to validate codes and establish CFD as a viable tool for wind energy engineering design, along with scale down experiments, and reduce testing on predesign parameters. Several types of numerical models with different levels of complexity have been used to simulate the flow field around and in the wake of wind turbines [12]. Simms et al. [13] from NREL performed comparisons between predicted and measured integral variables of the NREL Phase VI turbine under different operating conditions. They concluded for the no-yaw, steady–state, no–stall cases, turbine power predictions ranged from 25% to 175% of measured values depending on the fidelity of the numerical model. According to Simms et al., among different numerical models investigated in this report, the 3D incompressible Navier-Stokes

182   Hierarchical Methodology for the Numerical Simulation of the Flow Field around and
in the Wake of Horizontal Axis Wind Turbines: Rotating Reference Frame,
Blade Element Method and Actuator Disk Model

CFD model showed the most promising numerical results compared to experimental results. The focus of this work is also on solving 3D Reynolds-Averaged Navier-Stokes (RANS) equations to simulate the flow around specific turbine blade geometries. Sørensen et al. [9] solved the RANS equations on the NREL Phase VI, using curvilinear coordinates on the exact geometry of the blade. They reported very good agreement on shaft torque, flap and edge moments, and pressure distribution between numerical and experimental data for various Tip Speed Ratios (T.S.R = 5.95, 4.18, 3.21, 2.77, 2.07, 1.66) and Reynolds numbers ($5.45 \ 10^6$ to $1.90 \ 10^7$). However, for very low T.S.R (i.e. 1.66) they reported a 25% underprediction in numerical data compared to experimental data. This disagreement was due to massive flow separation along the full span of the blade in that operating condition. The Rotating Reference Frame (RRF) was used by Carcangiu [11] for a full scale 3D RANS numerical study of the Nordtank NTK 41/500 and NREL Phase VI wind turbine designs. Power and thrust coefficients compared favorably against experimental and previous numerical data. This work investigated the wake of these two turbines, specifically focusing on the generation of tip vortices, the effect of blade tip geometry on their structure and the issues of CFD simulations in capturing them.

Although RRF modeling provides details of the flow field around the blades and in the near wake, it requires complex meshing and is computationally expensive. As a result, simpler and numerically less expensive formulations have been developed to calculate HAWT flow field behavior and performance. One of these simplified formulations is based on Blade Element Theory. Glauert [14] presented this formulation while giving credit for its development to S. Drzewiecki. Early on, use of this model focused on the flow field around helicopter blades. Originally, Laith and Rajagopalan [15] developed a numerical method to analyze the rotor-airframe interaction. This method applied the concept of momentum source, calculated based on the Blade Element Theory, to the Navier-Stokes equations to model the rotor-airframe interaction. This work showed that the newly proposed method models the wake of the rotor properly and the results are in a good agreement with experimental data. In the last decades, this method has been applied extensively to modeling wind turbine performance and wake-wake interaction of multiple turbines in farms [16, 17]. Recently, there have been several studies focused on developing more advanced numerical methodologies based on the Blade Element Model (BEM) [18–19]. Parallel to this process, many studies have focused on improving the accuracy of the available methodologies, while maintaining the computational cost at the same level [20–21]. Another simplified model, the Actuator Disk Model (ADM), is based on Linear Momentum Theory. This formulation was introduced by Froude [22] over a century ago and it has become an important tool for simplified investigation of the flow field in horizontal axis wind turbines. Numerous extensions on this simple model have been developed from the early 90s to the present time [23–26]. Van Kuik [23] presented a comprehensive study on the rotor representation using the actuator disk concept. The numerical results were compared against the experimental results, and strengths and weaknesses of the ADM were discussed. Mikkelsen [24] combined the ADM and 3D actuator line technique with the incompressible Navier-Stokes equations to model the flow field through a wind turbine rotor under various operating conditions. The numerical results were compared against theory and the strengths of the ADM were highlighted. However, both of the abovementioned works don't present a detailed and direct comparison of the ADM with other alternative numerical methods for modeling the flow field around the rotor of a wind turbine.

As the pioneering research referenced above sheds light on the turbulent flow physics in wind turbines, improving the understanding of the fundamental physical processes responsible for single turbine performance and environmental effects (wake-turbine and wake-wake interactions), the need has grown for faster numerical models that can provide a quick turn-around solution for certain aspects of single turbine or array design optimization.These simpler models, BEM and ADM, are able to capture, with sufficient accuracy, the key physics that determine integral variables, such as drag and power, but not necessarily reproduce every detail of the flow on the turbine blades or in the near wake. High fidelity numerical models can be used for comparison with simpler models at a few key operational points and from that comparison, establish the range of validity and accuracy of fast turn-around models. This type of comparisons between numerical models with different levels of complexity to evaluate their range of applicability represents a gap in our current understanding. Hence, the main objective of the work presented here is to compare full-blade geometry-resolving models with simpler rotor models, within the framework of 3D RANS

computational simulations. This evaluation is necessary to assess the applicability of computational models to large-scale problems in wind energy like siting and array design. Other open questions in renewable energy can benefit from this same hierarchical methodology for computational simulation: these models can also be applied to Marine Hydrokinetic (MHK) energy conversion devices such as Horizontal Axis Hydrokinetic Turbines (HAHT).

The background for the three models used in the simulations is presented in Section 2, with the actual numerical setup discussed in Section 3. Section 4 includes the results from our three models: a full 3D RANS numerical model of the NREL Phase VI wind turbine using the Rotating Reference Frame (or Single Reference Frame, SRF), and simulations using BEM and ADM of the flow field in the wake of the NREL Phase VI turbine, under the same operational parameters. As mentioned earlier, the NREL Phase VI turbine underwent testing for a wide range of TSR values. Turbine operation under very low and very high TSR values resulted on significant flow separation over the span of the blade. RANS solutions of separated flows over progressively increasing angle of attack geometries, including our SRF turbine model, can not reliably predict the separation onset and, therefore, the span of the turbine blades that is operating under these conditions. The simulations in this work are conducted under conditions that minimize flow separation on the blade in order to ensure the highest level of accuracy of the simulation with all three models. This allows for an equitable comparison of the SRF turbine model that has no empirical input and needs to predict separation from the RANS equations, against BEM and ADM where experimental data on lift and drag coefficients or induction factors enables them to produce estimates of performance over the whole range where experiments are available, without truly resolving the detached flow on the blades. We also compare our results against previous numerical studies [27, 9, 28]. The results of the two lower fidelity models (BEM and ADM) are compared against the SRF simulation, with the goal of understanding to what degree different numerical models can simulate HAWT performance and flow field characteristics. The summary of the three methodologies, with a critical analysis of their capabilities and trade-offs, along with the key conclusions in terms of the physics are included in Section 5.

2 METHODOLOGY
2.1. Single Rotating Reference Frame Model
In the SRF technique, the flow field around a Horizontal Axis Wind Turbine (HAWT) blade is simulated in an alternative reference frame that rotates at the constant angular speed of the turbine rotor. Generally, in a laboratory inertial reference frame, the flow field is unsteady (figure 1-a), but it is possible to perform calculations in a non-inertial reference frame, rotating with the turbine blades, where the flow is steady (figure 1-b).

In this formulation, the effect of rotation is input into the equations of fluid motion by adding body forces that represent the inertial effects associated with the centrifugal and Coriolis accelerations felt by the fluid in its motion with respect to the non-inertial reference frame. The addition of these body forces and the transformation of the velocity components due to changing the frame of reference in the equations of motion are as follows:

$$\frac{\partial \rho}{\partial t} + \nabla.\rho \vec{v}_r = 0, \tag{1}$$

$$\frac{\partial}{\partial t}\left(\rho \vec{v}_r\right) + \nabla.\left(\rho \vec{v}_r \vec{v}_r\right) + \rho\left(2\vec{w}\times\vec{v}_r + \vec{w}\times\vec{w}\times\vec{r}\right) = -\nabla p + \nabla.\bar{\bar{\tau}}_r + \vec{F}, \tag{2}$$

$\vec{v}_r$ is the velocity relative to the rotating reference frame and is equal to ($\vec{v} - \vec{\omega}\times\vec{r}$), where $\vec{v}$ is the absolute velocity and ($\vec{w}\times\vec{r}$) is the velocity due to the rotation of the reference frame. In equation (2), ($2\vec{w}\times\vec{v}_r$) is the Coriolis acceleration and ($\vec{w}\times\vec{w}\times\vec{r}$) is the centripetal acceleration, which are added as body forces to the conservation of momentum equation [29]. In order to implement this formulation in the numerical scheme, the entire fluid domain is set to move with a constant rotational velocity around the axis of rotation. The inputs of rotational velocity, rotational axis origin and rotational axis direction provide all the required information to pose the

184   Hierarchical Methodology for the Numerical Simulation of the Flow Field around and
in the Wake of Horizontal Axis Wind Turbines: Rotating Reference Frame,
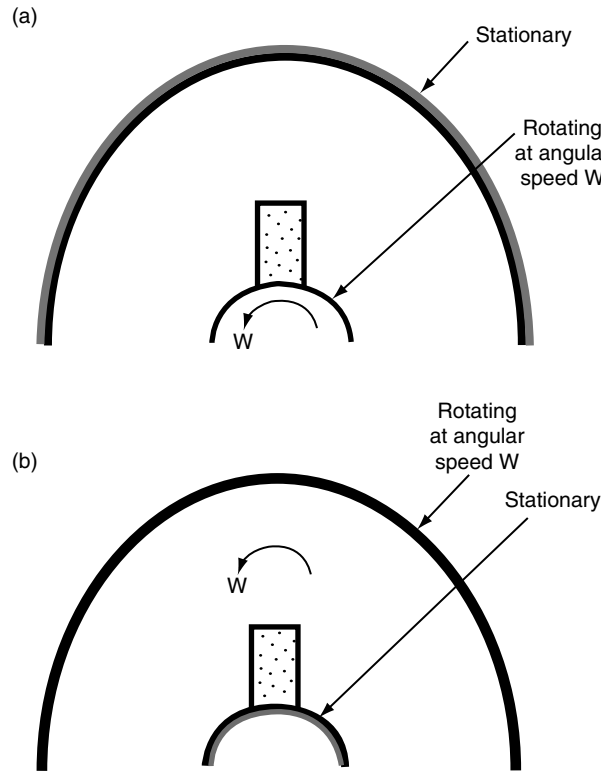Blade Element Method and Actuator Disk Model

Figure 1. Front view of a computational domain with a turbine blade inside. (a) the turbine blade is rotating with respect to the stationary frame (unsteady flow field). (b) the blade is stationary and the frame is rotating with respect to the blade (steady flow field)

problem based on equations (1) and (2) in the framework of the RANS equations, implementing the SRF turbine model.

This method renders an unsteady problem in a fixed reference frame into a steady problem with respect to the rotating reference frame. This allows the problem to be integrated using a stationary grid and to avoid the complexity and stiffness associated with rotating mesh simulations. The trade-off in the use of this method is that it requires an axisymmetric domain and boundary conditions. This requirement has to be taken into account in selecting the turbulence closure models, since many existing models compute Reynolds stresses in a way that is not independent of the rate of rotation and therefore will not perform well in a rotating reference frame.

2.2. Blade Element Model (BEM)

The BEM represents a step down in complexity for simulation of the flow around rotating blades. This model is based on Blade Element Theory [30] and models the presence of the rotating turbine blades in the computational domain via a fluid sub-domain that occupies the disk swept by the turbine blades over a complete revolution [15]. In the BEM, the blade span is sectioned from root to tip, and the lift and drag forces on each section are computed based on the local angle of attack (AOA), chord length and airfoil shape. The BEM simulates the effect of the rotating blades by imposing a body force calculated on the fluid equal in magnitude, but opposite in sign, to the lift and drag on each blade element averaged over a full revolution, inside the rotor disk domain (i.e. fluid sub-domain). Eq. (3) shows the formulation of the sectional lift and drag forces.

$$f_{L,D} = c_{L,D}(\alpha, \text{Re}) \ . \ c(r\,/\,R). \ \frac{\rho.V_{tot}^2}{2}. \tag{3}$$

This equation uses the value of the lift or drag coefficient, $c_{L,D}$ to calculate the body forces applied in the BEM. These coefficients come from a lookup table that contains the values as a

function of AOA (α) and Reynolds number (Re) for the blade airfoils. $c\,(r\,/\,R)$ is the chord length of the blade section, ρ is the air density and V_{tot} is the air velocity relative to the blade. The lift and drag forces calculated for each element are averaged over a full blade revolution to calculate the equivalent source term in each cell of the numerical discretization [20]. The full numerical implementation of the BEM in a numerical RANS solver requires inputs that can be divided into two main groups: the size, number and pitch angle of the wind turbine blades; and the geometrical specifications of the blade sections along its span, with the corresponding lift and drag coefficients look-up tables for each blade element. Each look-up table defines the characteristics of the different airfoil sections along the blade span. With these inputs, the body forces at each blade section are calculated and averaged over the swept area of the blade. The body forces are included into the RANS equations to model the effect of wind turbine rotating blades, in an iterative process. A detailed characterization of this process, with specific examples of input values, is given in [31].

This formulation eliminates the need for creating the actual geometry of the turbine blades and a high resolution mesh around it in the computational domain[1]. The aerodynamic parameters are calculated by the BEM based on the simulation of the induced flow at the turbine and the rotational speed of the turbine input into the simulation. The body forces are applied to the flow and the aerodynamic force calculation is iterated until the induced flow calculation is consistent with the aerodynamic force calculation across the rotor disk.

2.3. Actuator Disk Model (ADM)

The ADM represents the turbine as a sink of momentum (drag) and energy (extracted plus dissipated) where the aerodynamic effect of the turbine rotor is represented by a pressure discontinuity over an infinitely thin disk occupying the swept area of the rotor [32]. In the numerical solver's implementation of ADM, the turbine disk is modeled as a porous material that supports pressure but not velocity discontinuities. Eq. (4) simulates the actuator disk effect as the pressure drop through a porous material. The modeled pressure difference across the porous media integrated over the rotor swept area equals the drag on the turbine. Using a combination of Darcy's law and an additional inertial loss term in eq. (4), the coefficients for the porous material in the turbine disk are calculated so the conservation of momentum and energy are satisfied in an integral sense. The turbine presence is thus input into the flow field, creating a momentum deficit that evolves into the far wake.

$$\Delta p = \left(\frac{\mu}{\alpha} v + C_2 \frac{1}{2} \rho v^2 \right) \Delta m. \tag{4}$$

Equation (4) provides the pressure drop as a function of the face permeability of the media, α, and the pressure jump coefficient, C_2. μ is the fluid dynamic viscosity, v is the velocity normal to the porous face and Δm is the thickness of the media. Based on the turbine efficiency (induction factor) as a function of wind speed, assumed to be known under the operating conditions from either experiments or higher fidelity numerical models (i.e. SRF or BEM), α and C_2 are evaluated to estimate the pressure drop across the porous media. A second order polynomial fit of the pressure difference as a function of the velocity normal to the porous face is derived, based on either experimental or numerical data of the pressure difference across the porous disk and the corresponding velocity normal to the disk for different operating conditions[2]. Equating the coefficients of the resultant second order polynomial to the terms in eq. (4) will set the coefficient for the porous media that represent the turbine. A more detailed description of the parameter fitting and input process for ADM is provided in [31].

The resulting representation of the turbine is a very simple but robust model that can calculate the flow around a wind turbine and in the far wake with very low computational cost, typically an order magnitude less than BEM computations. Limited accuracy and the requirement for significant information on turbine performance for some operational conditions are the main draw-backs in this model.

---

[1]Due to the lack of a blade geometrical model the name Virtual Blade Model (VBM) is also used for this rotor representation. Furthermore, this model reduces the mesh count, man-hours required in its generation and computational cost by between 10 and 100 times with respect to blade-resolving methods

[2]For the numerical data, the relationship between the pressure difference and velocity normal to the porous disk is defined by the Linear Momentum Theory (LMT).

186   Hierarchical Methodology for the Numerical Simulation of the Flow Field around and
in the Wake of Horizontal Axis Wind Turbines: Rotating Reference Frame,
Blade Element Method and Actuator Disk Model

3. NUMERICAL MODEL SETUP AND COMPUTATIONAL DOMAINS

3.1. Turbulence model

Numerical simulations were performed with a commercial finite volume code, FLUENT 12.0 (ANSYS Inc., Cannonsburg, PA), by solving the RANS equations with a turbulence model to provide closure for the Reynolds stress term. Among the turbulent closure models that have been used for flow field simulation in HAWTs, this work focuses on two commonly used turbulence models: Spalart-Allmaras (SA) with a strain/vorticity-based production term, and Shear Stress Transport (SST) $k - w$. SA is a one-equation closure model originally developed for high-speed aerodynamic flows. SST $k - w$ is a modification of the original $k - w$ model that overcomes its limitation for capturing the turbulent boundary layer around the blade. Additionally, far from the boundary layer region, this model transitions to the $k - \epsilon$ model to capture the free-shear flow region in the far wake. According to the fundamental differences in modeling the turbulence in the flow field through these two models (i.e. one equation versus two-equation), it is expected that these models simulate the near and far wake region of the turbine differently. Performing a detailed comparison between these two models will provide the opportunity to highlight their strengths, weaknesses and range of applicability, and to present a general methodology to model the flow field around and in the wake of a HAWT rotating blades.

In the SA model, developed mainly for high-speed aerodynamics [33], the effective turbulent viscosity is considered as a dependent variable governed by a rate equation. Similarly to any other scalar in the flow, the effective turbulent viscosity is transported by convection and diffusion. The effects of production, convection, diffusion and dissipation are included in the model, based on the physics of the problem, in this case, wall-bounded turbulence developing along the blade, and adjusted with semi-empirical coefficients [33]. Considering the physics of the turbulent flow, within the framework of the model, if the production term depends solely on vorticity ω_{ij}, then the eddy viscosity is drastically overproduced in vortex cores (i.e. the tip vortices or the coherent structures shed in the wake within the first few radii downstream of the blades). Hence, for an accurate flow field simulation, a correction in the production term becomes necessary. We implement the correction using the strain/vorticity-based production proposed by [34]:

$$S \equiv \left\| \Omega_{ij} \right\| + C_{\text{prod}} \min\left(0, \left\| S_{ij} \right\| - \left\| \Omega_{ij} \right\|\right). \tag{5}$$

where $C_{\text{prod}} = 2.0$ is a constant model parameter, and $||\Omega_{ij}||$ and $||S_{ij}||$ are the norms of the vorticity and rate of strain tensors, respectively.

According to eq. (5), the production term will be reduced in regions where the vorticity is higher than the rate of strain ($||\Omega_{ij}|| > ||S_{ij}||$), such as the tip vortex cores and in coherent structures in the near wake region. In regions where vorticity and rate of strain are of similar magnitude ($||\Omega_{ij}|| \approx ||S_{ij}||$), there is no effect as the correction term goes to zero.

The second model used is the SST $k - w$, a modification of the model based on the transport equations for turbulence kinetic energy, k, and specific dissipation rate, w, developed by Menter [35]. Menter developed the SST $k - w$ to take the best features from the $k - w$ and $k - \varepsilon$ models in their respective regions of applicability: the calculation of the turbulent viscosity is modified to account for the transport of the principal turbulent shear stress to include the addition of a cross-diffusion term in the w equation, and to ensure that the model equations behave appropriately in both the near-wall as well as far-field regions. In near wall regions, the blending function tends toward zero (i.e. the standard w equation), whereas far from the walls, it tends toward unity (i.e. the standard ε equation) [36]. Table 1 summarizes the constant values for two turbulence models, Spalart-Allmaras (SA) and SST $k - w$, that are used in this work to simulate the flow field around and in the wake of a HAWT.

3.2 Choice of turbine geometry

In this study, we used the National Renewable Energy Laboratory (NREL) Phase VI turbine because it is a well understood HAWT that has been extensively studied, including full-scale testing in the 80'x120' NASA AMES wind tunnel [4]. The detailed performance and pressure coefficient data from that experimental campaign allows for careful validation of the simulation results [28]. Other numerical studies in the archival literature, matching our geometry and operating conditions, were used to validate our results [27, 37]. Table 2 shows the specifications of the NREL Phase VI turbine.

Table 1. Constant values for the Spalart-Allmaras (SA) and SST $k - w$ turbulence model

				SA			
C_{b1}	C_{b2}	C_{v1}	C_{w2}	C_{w3}	C_{prod}	$\sigma_{\tilde{v}}$	k
0.1355	0.622	7.1	0.3	2	2	0.667	0.4187
			k − w SST				
α_∞^*	α_∞	β_∞^*	ζ^*	M_{t0}	a_1	$\beta_{i;1}$	$\beta_{i;2}$
1	0.52	0.09	1.5	0.25	0.31	0.075	0.0828
$\sigma_{k,1}$	$\sigma_{k,2}$	$\sigma_{w,1}$	$\sigma_{w,2}$				
1.176	1	2	1.168				

Table 2. NREL Phase VI turbine specifications.

Number of Blades	2
Primary Blade Airfoil	S809
Rated Power [kW]	20
Rotor Diameter [m]	10
Rotor Speed [rmp]	72
Wind Speed [m/s]	6.8

3.3. Computational domain, boundary conditions and numerical settings
3.3.1. Single rotating reference frame model

The computational domain for the SRF simulations is a half cylinder (due to the symmetry of the two-bladed rotor) 24 blade-radii long and six blade-radii in diameter. The domain is broken into three main blocks for meshing, as shown in figure 2(a). The volume upstream of the turbine is 9 radii long. The blade geometry is located in the middle block, including a high-resolution structured C-mesh around the blade that provides an accurate solution to capture the turbulent boundary layer along the span of the blade. The third block, 13.5 radii long, is the volume downstream of the turbine, where the wake develops. The boundary conditions are constant velocity ($V_\infty = 6.8$ m/s) at the inlet and uniform pressure ($P = P_\infty$) at the outlet. Cyclic-periodic boundaries are prescribed on the symmetry plane (the half cylinder plane) of the domain to simulate blade rotation. The domain's top cylindrical wall is modeled with a shear-free wall boundary condition (no stress in the tangential directions and no flow-through in the normal direction) to simulate the high Reynolds number wind tunnel conditions.

A close-up of the middle block section is shown in figure 2(b) to highlight the details of the structured C-mesh around the blade. The C-mesh around the blade section has 110 cells. 48 cells were created on lines perpendicular to the chord, with higher resolution near the surface of the blade to capture the development of the turbulent boundary layer in this region (first length = 2.1 mm). 73 cells were distributed along the blade span from root to tip, with finer mesh near the tip to capture the blade-tip vortex shedding. At the tip, an unstructured mesh block was added, with 1200 pave quadrilateral cells over the tip surface and 40 elements along the span, from the tip of the blade to the top of the channel. In order to avoid highly skewed elements at the tip of the blade, the trailing edge had to be manually modified [31]. Figure 2(b) shows the blade geometry and grid structure used to grow the cells away from the blade and into the wake to keep the cell count and the computational cost of the simulations within reasonable bounds. Figure 2(b) also highlights how the hub was simplified to match the limitations of axisymmetric boundary conditions imposed by the use of the SRF model. The original geometry for the hub of the NREL Phase VI turbine is complex, not axisymmetric and with poor aerodynamics. This unconventional geometry makes it impractical to include the original hub in any computational study of the NREL Phase VI NASA AMES tests. To avoid any potential uncertainty in the turbine wake results by simplifying the original hub geometry, the hub was removed. The blade geometry in our simulations, starts at the point where its cross-section takes the shape of the S809 airfoil, reducing the uncertainty about the blade root geometry. A free stream velocity of 6.8 m/s and angular velocity of 72 rpm are chosen as operating conditions,

188   Hierarchical Methodology for the Numerical Simulation of the Flow Field around and
in the Wake of Horizontal Axis Wind Turbines: Rotating Reference Frame,
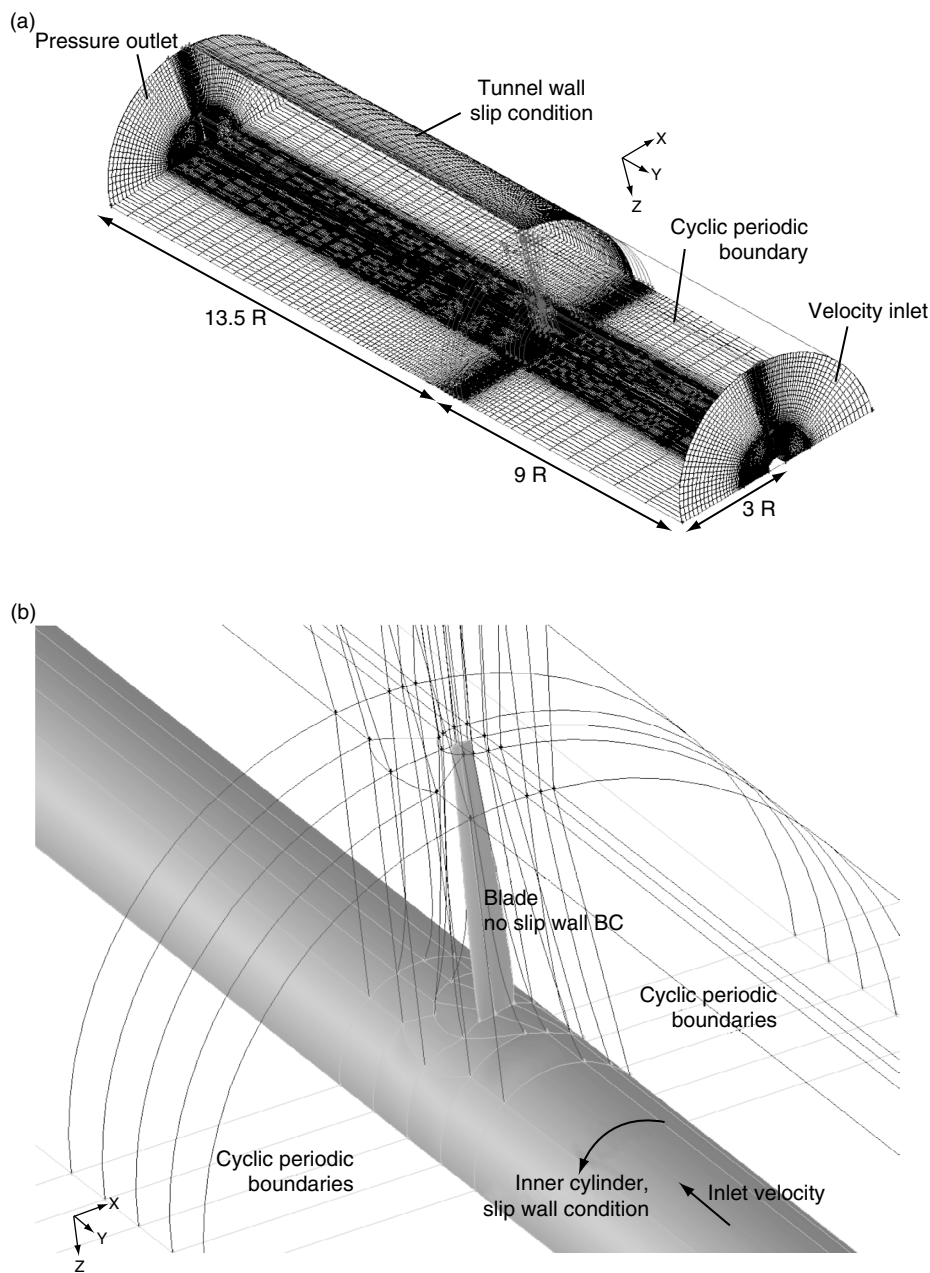Blade Element Method and Actuator Disk Model

Figure 2. (a) SRF full computational domain (b) zoom-in of the middle block including the actual geometry of the NREL Phase VI blade

from all the experimental values tested by NREL in the AMES Wind Tunnel, in order to minimize separated flow in our simulations.

3.3.2. Blade element model and actuator disk model

The BEM computational domain is created to match the SRF simulation, but is not limited by the use of cylindrical symmetry. This provides the opportunity to have exact comparisons between BEM and SRF results, while also allowing non-axisymmetric boundary conditions (i.e. a sheared inlet velocity profile or a bottom wall boundary condition) in more realistic simulations once the methodology has been validated. The BEM computational domain is similar to the SRF domain, as shown in figure 3. The first and third blocks are identical to the SRF's. The middle block includes the rotor disk, shown in figure 3, where body forces act on the fluid inside the disk to model the effect of the rotating blades. These momentum sources are calculated for each cell in the disk based
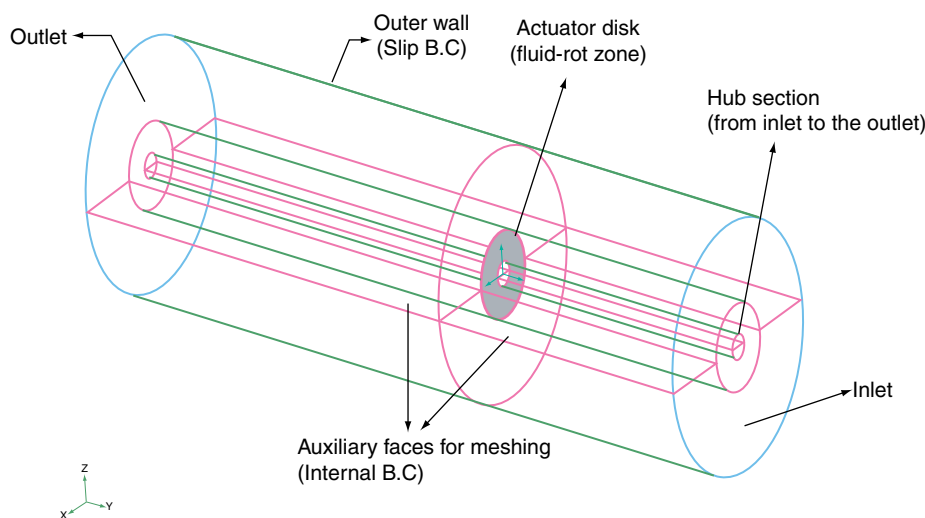
Figure 3. BEM and ADM domain and its boundary conditions

Table 3. Specifications on numerical settings and discretization in all three models (SRF, BEM and ADM)

Solver Type	Pressure-Based
Turbulent Models	Spallart-Allmaras or SST $k - w$
Pressure-VelocityScheme	SIMPLE
Discretization of Gradient	Green-Gauss Node Based
Discretization of Pressure	Second Order
Discretization of Momentum	QUICK
Discretization of Turbulent Viscosity	Second Order Upwind

on the solution for the flow velocity relative to the blade and the lookup table for the lift and drag coefficients, chord length, pitch and twist angle of segments along the blade span. The boundary conditions for inlet, outlet and side walls are all set exactly as described for the SRF, so the comparison between the simulations can be established. We do not use periodic boundary conditions at the horizontal planes in the middle of the domain, but rather use them as auxiliary faces in the meshing process.

The computational domain for the ADM is the same as the BEM domain (figure 3). The difference is in the rotor disk located in the middle block of the domain. As discussed earlier in section 2.3, the ADM models the effect of the turbine via a porous disk. The domain that occupies the volume swept by the blade is therefore defined as a porous material in the simulation. Two coefficients that define the porous material are matched [32] so that the pressure drop and induction factor behave consistently with turbine performance.

Table 3 summarizes the details of the numerical settings and discretization used to model the flow field around turbine blades in all three different models.

4. RESULTS AND DISCUSSION
In the study of the flow field around wind turbine blades, the turbulent wake generated by the power extraction is an important physical phenomenon. Therefore, a good understanding of the physics of this flow and its complete characterization is critical to the optimization of the energy extraction and minimization of environmental effects in large arrays. As discussed earlier, numerical modeling is one of the tools to characterize the wake of HAWTs. Figure 4 shows a hierarchy of the three numerical models, explained in section 2, for performance and wake characterization of HAWTs. As shown in figure 4 each of these models takes inputs in different forms and provides outputs with

190   Hierarchical Methodology for the Numerical Simulation of the Flow Field around and
in the Wake of Horizontal Axis Wind Turbines: Rotating Reference Frame,
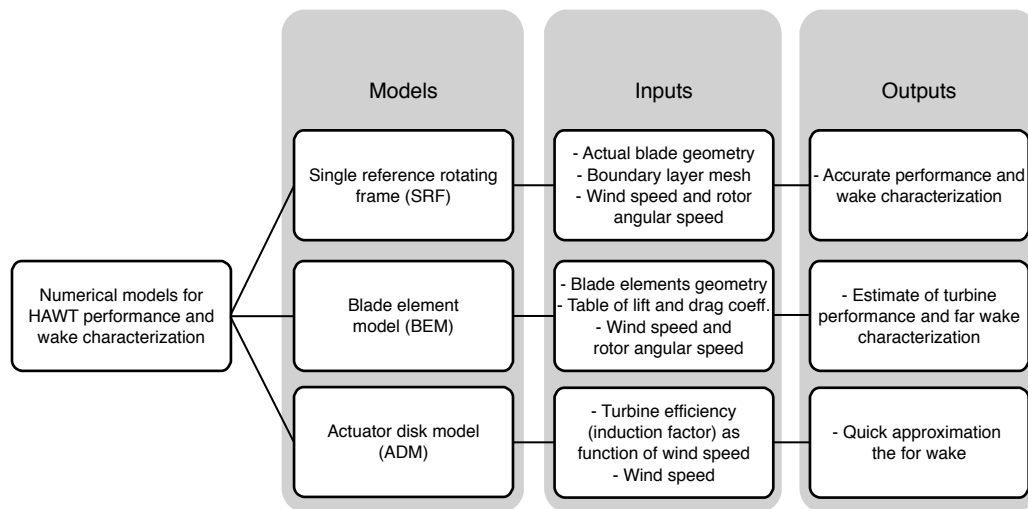Blade Element Method and Actuator Disk Model

Figure 4. Diagram of hierarchy of three numerical models, their inputs and outputs

different level of accuracy. The model with the highest level of fidelity (SRF) requires a lower number of inputs but has more complex nature, such as a full 3D model of the rotor and a high-resolution mesh at its surface and fluid volume domain around it. This high-resolution numerical simulation provides accurate results but demands high computational time and cost. The lower fidelity models (BEM and ADM) require a larger number of more specific inputs, such as an airfoil type and chord distribution chart and a simple mesh. The inputs of these models can be obtained from a few selected experiments or higher fidelity numerical simulations. These simpler models can then be used in modeling turbines over a wider range of parameters, or in larger domains that introduce other types of complexity (i.e. modeling a large array of turbines or turbines on complex topography) where experiments or high-fidelity simulations can not be realistically (or physically) carried out. This section describes the strengths, weaknesses, flexibilities and limitations of each model, by comparing their results against published experimental and numerical data, and against each other. Thus, it provides specific guidelines to carry out research and development of HAWT arrays, based on the desired outputs from the numerical model, and the available turbine inputs and resources.

The effort to capture the complex flow around turbine blades that give rise to the turbulent wake starts with resolving the flow in the boundary layer that develops along the rotating surfaces of the blades. Numerical simulations of this boundary layer require a specialized mesh, optimized to resolve the flow in this critical region, together with appropriate models in the context of the RANS equations and the limitations imposed on the spatial resolution by the high Reynolds numbers in this type of flows. The least expensive computational approach for this process is to start with the 2D reconstruction of the blade cross section before trying to model the fully 3D flow around a blade. In this effort, first a 2D simulation of the S809 airfoil, shown in figure 5(b), is used to investigate the structure and resolution of the mesh, the appropriate choice of turbulence models and numerical schemes to accurately capture the boundary layer around the airfoil. In the first set of results, all the boundaries shown in figure 5(a) are set to the velocity inlet except section BCD at the end of the C-mesh. This section is set to a pressure outlet. These boundaries are idealized since they do not represent the blade rotation. This first simulation set is used to determine the right level of mesh resolution and the influence of the choice of turbulence model.

This first set of numerical results, and the choices of mesh resolution and turbulence model in them, were validated against experimental and numerical studies. The predicted values of lift and drag coefficients as a function of angle of attack from 2D simulations were compared against other publicly available experimental and numerical data. A second set of 2D simulations, based on the actual horizontal cross section from the full 3D domain, shown in figure 7, were modeled with more accurate boundary conditions. In those simulations, the effect of blade rotation was introduced via periodic boundary condition and translational velocity. Those velocity conditions are critical in the
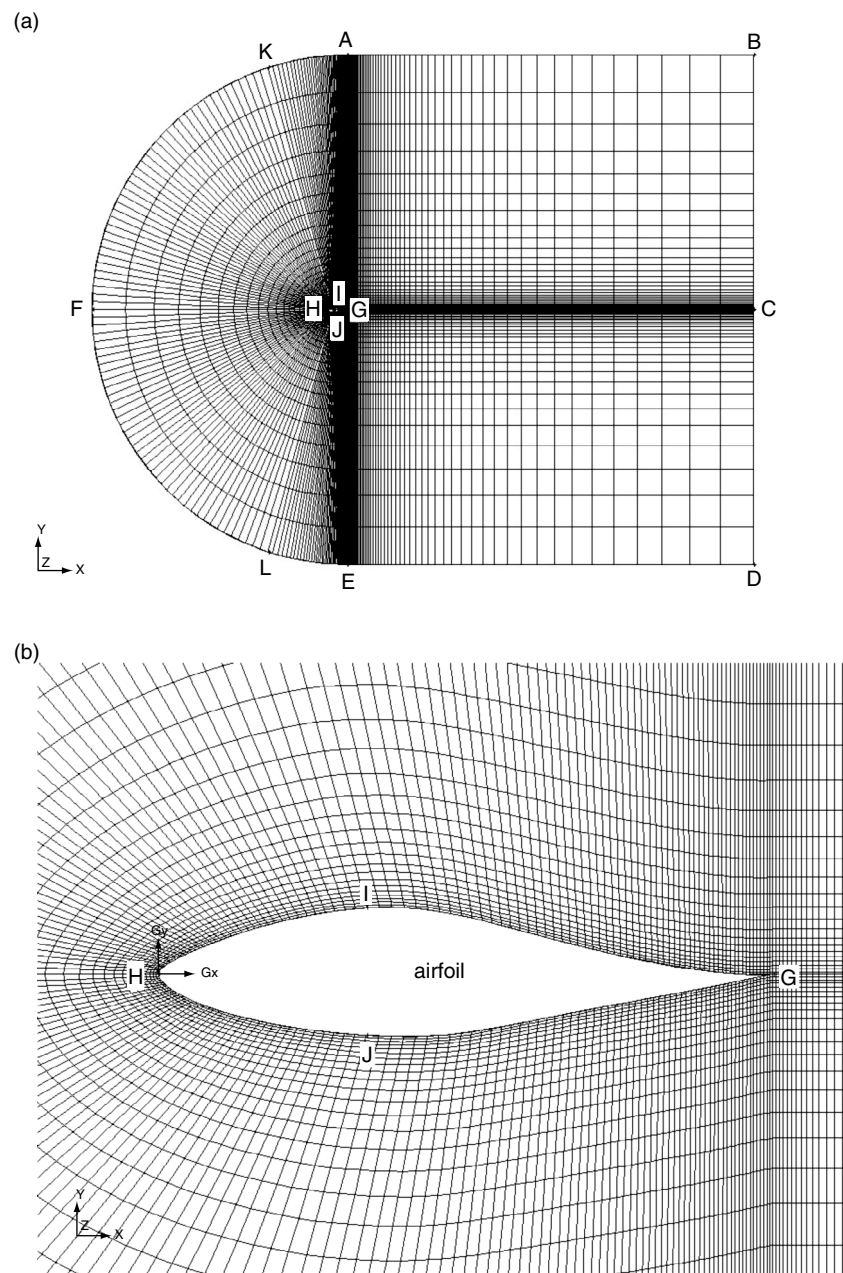
Figure 5. (a) 2D C-mesh around the S809 airfoil with idealized boundary conditions. (b) Zoom-in of mesh structure and resolution around the S809 airfoil

development of the turbulent boundary layer on the blade wall. The comparison of the predicted pressure coefficient at different radial positions along the blade span, against NREL experimental data provided validation that the structure and resolution of the mesh was appropriate. The 3D SRF simulations were all based on the mesh resolution and structure from those preliminary validation studies. The results of these three sets of simulations, as well as the simplified BEM and ADM models, are described in detail in this section.

4.1. 2D Result
Figures 5(a) and 5(b) show full and zoomed-in views of the mesh structure around the S809 airfoil. The chord length of the airfoil is 1 [m] and the Reynolds number approximately 10^6. Based on previous experimental studies, we matched these simulations to appropriate operating conditions.

192   Hierarchical Methodology for the Numerical Simulation of the Flow Field around and
              in the Wake of Horizontal Axis Wind Turbines: Rotating Reference Frame,
                                    Blade Element Method and Actuator Disk Model

In the first phase of 2D simulations, two turbulence models, SST $k-w$ and Spalart-Allmaras, are used with two different numerical schemes to capture the turbulent boundary layer around the airfoil. The first scheme uses a wall function model where the viscous sublayer and the buffer layer are not resolved by the numerical discretization. Instead, a semi-empirical formula is used within the first element of the mesh next to the wall to bridge the gap between the wall and the outer layer of the boundary layer. The wall function represents the effect of the unresolved layers in the behavior of the flow in the resolved regions, allowing for the calculation of mean velocity profiles, flow detachment, dissipation and mean shear on the wall [38]. The second scheme is the near-wall capturing approach, in which the turbulence model, applied to the interior of the domain, is modified to enable the boundary layer to be resolved with a high resolution mesh all the way to the wall [38]. In order to investigate the differences in accuracy of each wall treatment, lift and drag coefficients for a range of angles of attack with both the wall function and wall capturing approaches were calculated. Parallel to this investigation different mesh resolutions around the blade were examined in order to find the optimal combination of mesh resolution and wall treatment to represent the turbulent boundary layer dynamics. The results were compared against 2D RANS [27] and experimental results [37]. Figure 6 shows the comparison with our numerical results, using an optimal mesh resolution and two different wall treatments. As shown in figure 6, our simulations show good agreement with the literature, with the exception of SST $k-w$ combined with wall function approach, which underestimates the lift coefficient at different angles of attack. This simulation also showed poor convergence at angles of attack above 10°. On the other side of the spectrum, the combination of the 1-equation Spalart-Allmaras turbulence model and both the wall function model (y+ > 30) and the wall capturing approach (y + < 1) showed good agreement with previous studies. Convergence for all angles of attack (up to 16°) was smooth and fast.

In order to get one step closer to the full 3D model, the flow field was simulated in 2D horizontal cross sectional cuts from the full 3D computational domain with more realistic boundary conditions. These 2D sections were cuts at different radial positions, $\frac{r}{R} = 0.3$, 0.47, 0.63, 0.8 and 0.95, along the blade span. Figure 7 shows zoomed-in view and boundary conditions of the 2D mesh. As shown in figure 7, the airfoil is meshed with the C-mesh technique and the optimal mesh resolution, validated by the previous mesh resolution study (figure 5(a)). The right and left boundaries (see figure 7) are set to be periodic with a translational velocity set by the angular velocity and radial position of the section
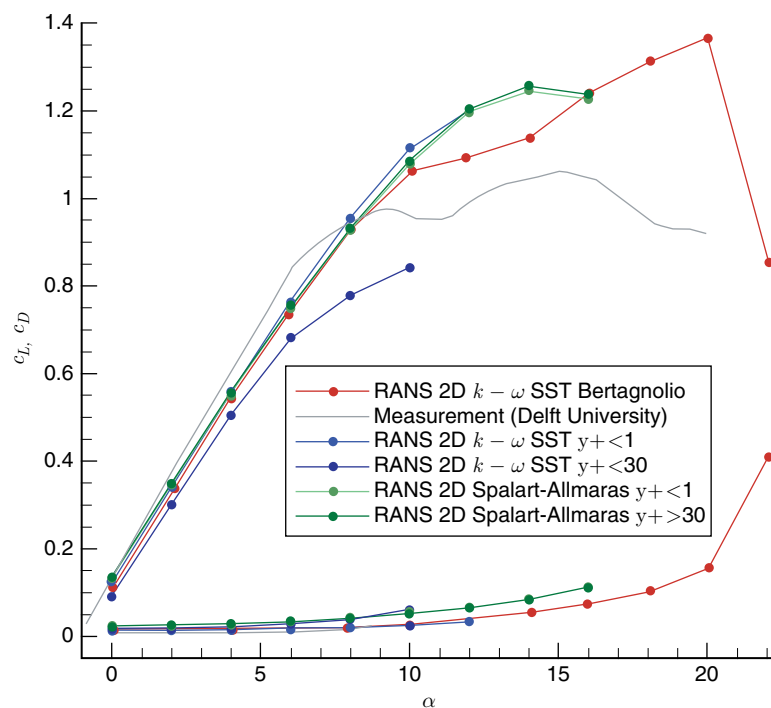

Figure 6. Comparison of lift and drag coefficient as a function of AOA results with previous experimental and numerical studies
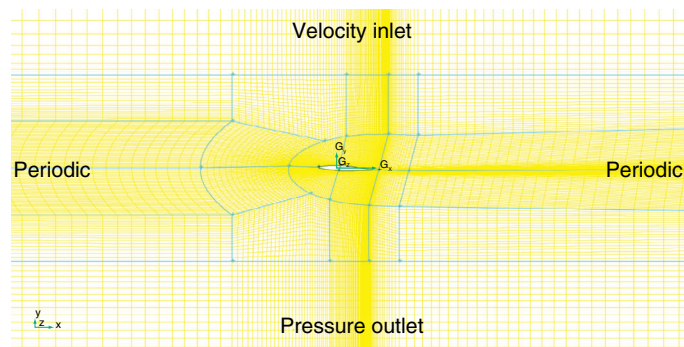
Figure 7. Zoomed-in view and the boundary conditions of the 2D domain cut from the 3D domain around the S809 airfoil, used in the second set of 2D simulations.

of the blade studied. This simulates the effect of blade rotation in the 2D simulations. The top and bottom boundaries are set to velocity inlet and pressure outlet respectively. These more realistic boundary conditions simulate the full 3D flow better than the uniform incoming wind speed in the previous 2D simulations. With this approach, the previous choice of mesh structure, grid resolution, turbulence model and numerical scheme are examined with conditions similar to the full 3D domain.

The pressure coefficients Cp at different radial positions $\frac{r}{R}$ along the blade span were compared against the NREL experimental data [4] in figures 8(a) to 8(c). The results present good agreement with the
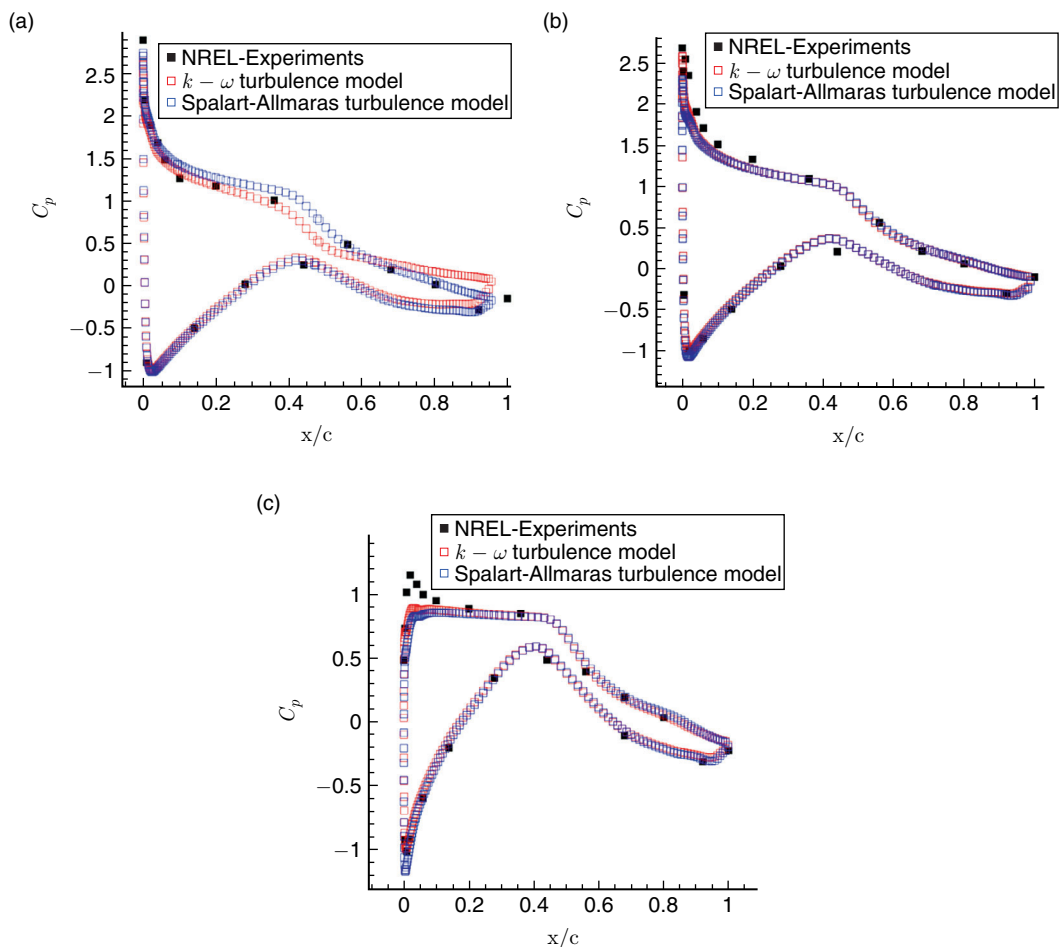

Figure 8. Comparison of computed pressure coefficients against NREL experimental data at radial positions (a) 0.30, (b) 0.47 and (c) 0.95

194   Hierarchical Methodology for the Numerical Simulation of the Flow Field around and
in the Wake of Horizontal Axis Wind Turbines: Rotating Reference Frame,
Blade Element Method and Actuator Disk Model

experimental measurements, except at the radial position nearest to the root, $\frac{r}{R} = 0.3$. At this position the disagreement becomes significant half way through the chord towards the trailing edge. This is the region where separated flow occurs. Furthermore, there is some inconsistency between the numerical and experimental values on the suction side of the airfoil close to the tip, $\frac{r}{R} = 0.95$, near the leading edge. This difference can be attributed to the generation of tip vortices at the blade tip. In this region, the flow becomes highly three dimensional and dominated by a strong coherent vortex, and the wall functions cannot accurately capture the exact details of the flow field (i.e. pressure field). Additionally, the flow acceleration in both the streamwise and spanwise directions, induced by the tip vortex, can lead to local inaccuracies due to the mesh, where further refinement may have been beneficial to better capture the details of the flow in this highly complex region. The values predicted by the simulations using the Spalart-Allmaras model generally show better agreement with the NREL experimental data. This model also had better numerical stability and convergence. At this point, the overall agreement between the computational results and the available experimental data validates our use of the C-mesh strategy and mesh resolution employed. It also leads to the conclusion that the Spalart-Allmaras turbulence model with a wall function approach is best to represent the boundary layer flow field around the airfoil with adequate accuracy and computational cost. This choice of models and parameter values were used in the 3D blade-resolving simulations (see figures 2(a) and 2(b)). The resulting grid resolution is consistent with previous numerical studies of the NREL Phase VI [9, 11].

4.2. 3D Results
4.2.1. Flow field around the blade and in the near wake
Figure 9 shows the streamwise velocity contours normalized with the undisturbed free stream velocity. These contours are plotted on $X - Z$ planes, perpendicular to the streamwise direction, along the computational domain.

The sequence of these planes starts upstream of the turbine, $\frac{y}{r} = -0.25$ (left corner top), and moves downstream, $\frac{y}{r} = 2.5$ (right corner bottom). As shown by the evolution of the velocity contours in the different panels, the flow starts to decelerate as the presence of the turbine rotor is felt through pressure changes. At the location of the blade, $\frac{y}{r} = 0$, acceleration of the flow on the suction side of the blade and deceleration on the pressure side are observed. At $\frac{y}{r} = 0$, high velocity "leaking" from the suction side to the pressure side, associated with the blade tip vortex formation in this rotating frame of reference, is also observed. This high velocity region, where the force imbalance between the pressure and suction side imparts vorticity to the fluid elements along the separatrix at the blade tip, is seen spilling over in a rotating motion imposed by the fluid domain displacement in this rotating reference frame (in a fixed reference frame the blade tip vortices trace counterrotating streaklines, with vorticity in the opposite sense). Moving further downstream, the tip vortex diffuses into the flow, becomes weaker and disappears, although the signature from the other blade comes into the domain before that happens ($\frac{y}{r} < 1$). As the distance downstream from the turbine increases, the velocity contours in the wake become more homogeneous. At about 1.5 radii downstream of the blade, the turbulent wake becomes axisymmetric. Observation of the axial symmetry of the flow in the wake only a few diameters (1–2) downstream of the rotor justify the use of less computationally intensive models such as BEM and ADM, which reproduce the flow field around the turbine and in the wake as axisymmetric, maintaining the integral values that characterize the turbine performance (thrust, torque and power) with good accuracy and at a much lower computational cost.

For a quantitative comparison between our numerical results and experimental data, Table 4 shows the comparison between the power extraction computed from our blade-resolving simulations and the NREL Phase VI experimental results [28]. The $k - w$ model overpredicts output power by 8.81%. The error in the power prediction by the Spalart-Allmaras model is smaller (4.50%). The root of this difference goes back to the fundamental differences in the formulation of the two turbulence models. This work uses a simplified blade geometry that cuts out the non-aerodynamic sections of the root, and therefore represents the blade starting at the point in the span where the blade section corresponds to the S809 airfoil. This simplification means that a small section of the blade is not simulated and therefore its contribution to the extracted power, although small, is not accounted for. A simulation using the the full blade geometry would reduce the difference between the SA results and the experiments, and increase the error if the k - w model were applied.
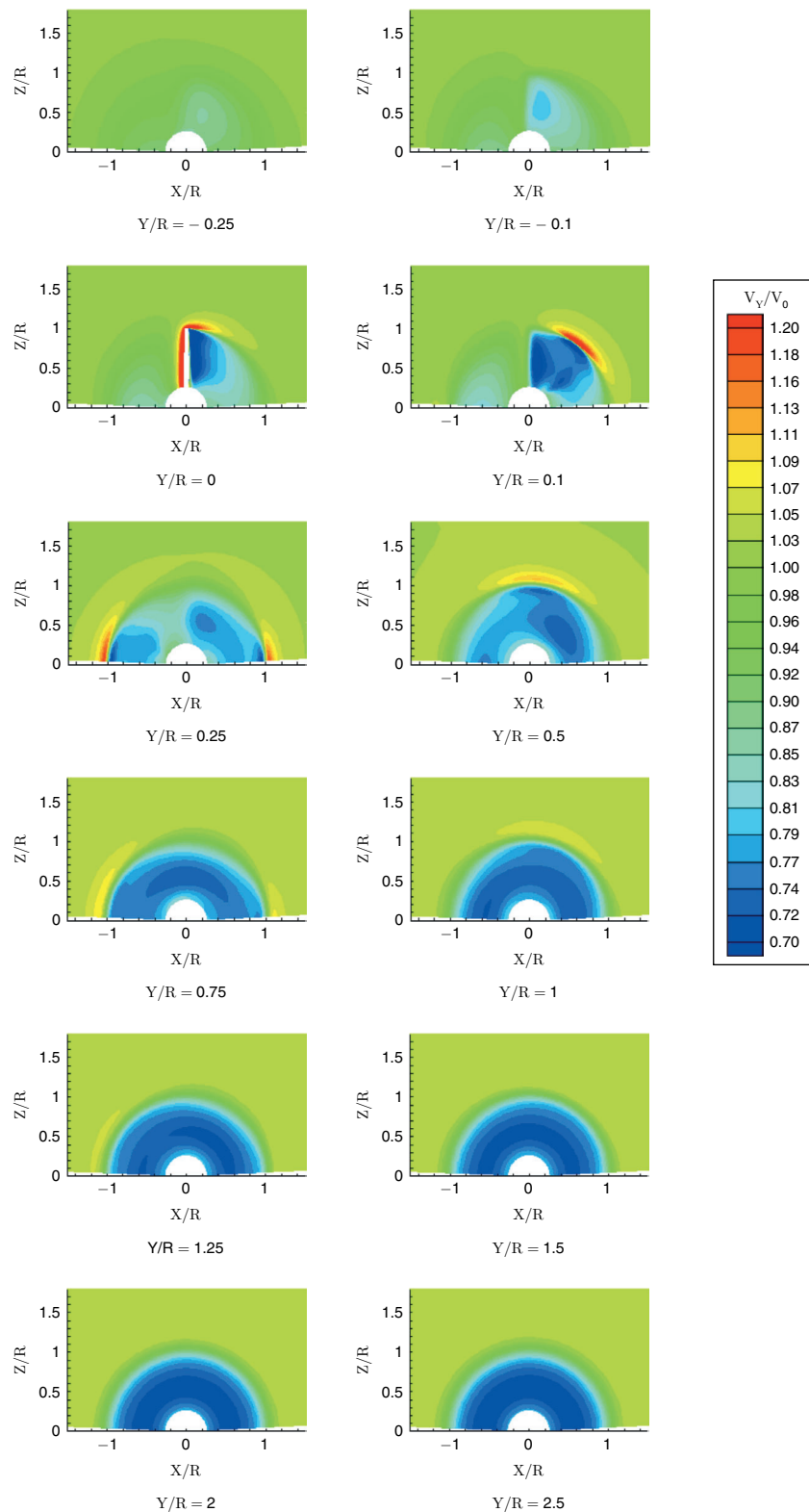
Figure 9. Normalized streamwise velocity contours on the Y-cuts plane along channel

Limited streamlines along the blade span are shown in figure 10. This result agrees well with the picture drawn by the pressure coefficients shown in figure 8. According to previous studies [9], the angle of attack for this operating condition varies between 5.11° and 7.54° . The limited streamlines here confirm that the flow is attached to the blade everywhere except for a small region at the root

196   Hierarchical Methodology for the Numerical Simulation of the Flow Field around and
                        in the Wake of Horizontal Axis Wind Turbines: Rotating Reference Frame,
                                          Blade Element Method and Actuator Disk Model

Table 4. Comparison between power computed via SA and SST $k - w$ models and NREL Phase VI experimental data

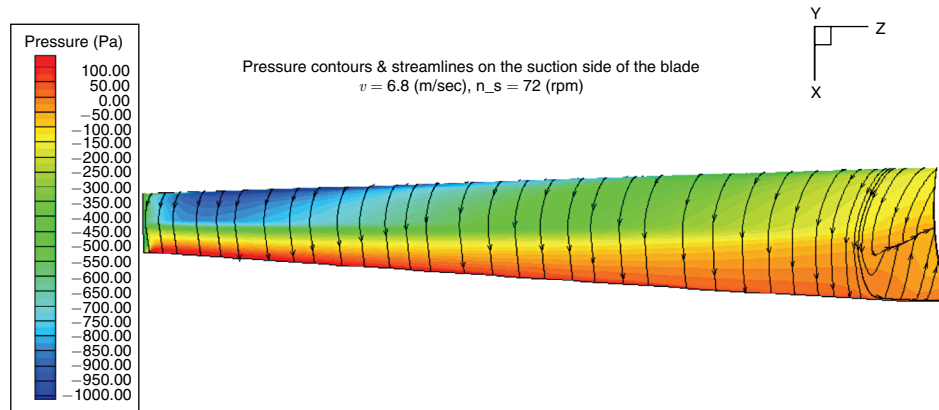|	Power [W]	Relative Error (%)
SRF using Spalart-Allmaras	5281	-4.5
SRF using $k - w$	6017	8.81
NREL Experiment	5530	—

Figure 10. Limited streamlines and pressure contours along the suction side of the NREL Phase VI wind turbine blade at a Tip Speed Ratio of 5.92

where the angle of attack reaches its maximum value. The presence of a very small separated region near the root can be observed in the pressure contours and the closed streamlines.

4.2.2 Flow field in the far wake

To visualize the wake due to the power extraction by the NREL Phase VI wind turbine, figures 11 (a), 11 (b) and 11 (c) show the streamwise velocity contours normalized with the free stream velocity on a $Y - Z$ plane (parallel to the free stream direction) in the middle of the channel. Superimposed with the contours, velocity profiles along $Y = constant$ lines (perpendicular to the flow direction) show the velocity deficit at different distances downstream of the rotor plane.

Figure 11(a) shows that the flow starts to decelerate as it approaches the rotor plane. Right behind the blades, in the near wake region, the flow becomes highly inhomogeneous and dominated by vorticity shed from the blade tip and root regions. This type of detail in the physics of the wake can only be simulated by the SRF model. Further downstream, however the turbulent wake starts to become axisymmetric. An interesting observation in this figure is that the helical blade-tip vortex generation is captured by the SRF model and visible in the form of small, discrete high-speed blobs near the tip of the blade, corresponding with the high velocity in the core of the tip vortices. Vortices are stronger closer to the blade, and get weaker as they travel about one radius downstream (the tip speed ratio is close to the value 2π at which the helical step of the tip vortex is exactly one radius per revolution) where the vorticity diffuses and eventually disappears in the flow. Velocity profiles, plotted in solid black lines, show the velocity deficit in the wake of the turbine.

The flow field simulated via the BEM is shown in figure 11(b). The general fluid mechanics of the flow, such as flow deceleration or the shape and velocity deficit of the turbulent wake, accurately simulated by this model, is in good agreement with results from the SRF model. However, there are some differences between these results that need to be considered. The first difference is that the BEM cannot capture the details of the flow right after the blade passage, since it is averaging the aerodynamic effects of the blade over the whole area of the disk. Therefore, the turbulent wake has an axisymmetric shape from the start. The second difference is that in modeling the vortex formation at the tip of the blade, the BEM predicts a continuous crown of vorticity, not
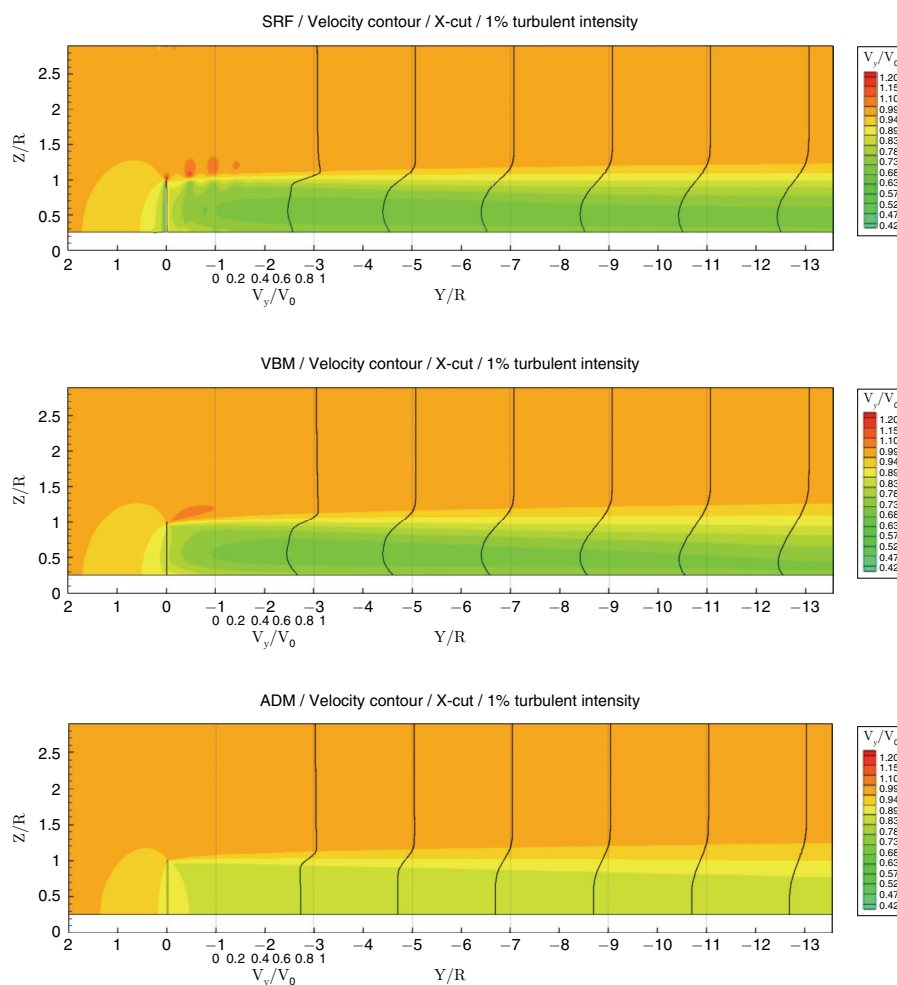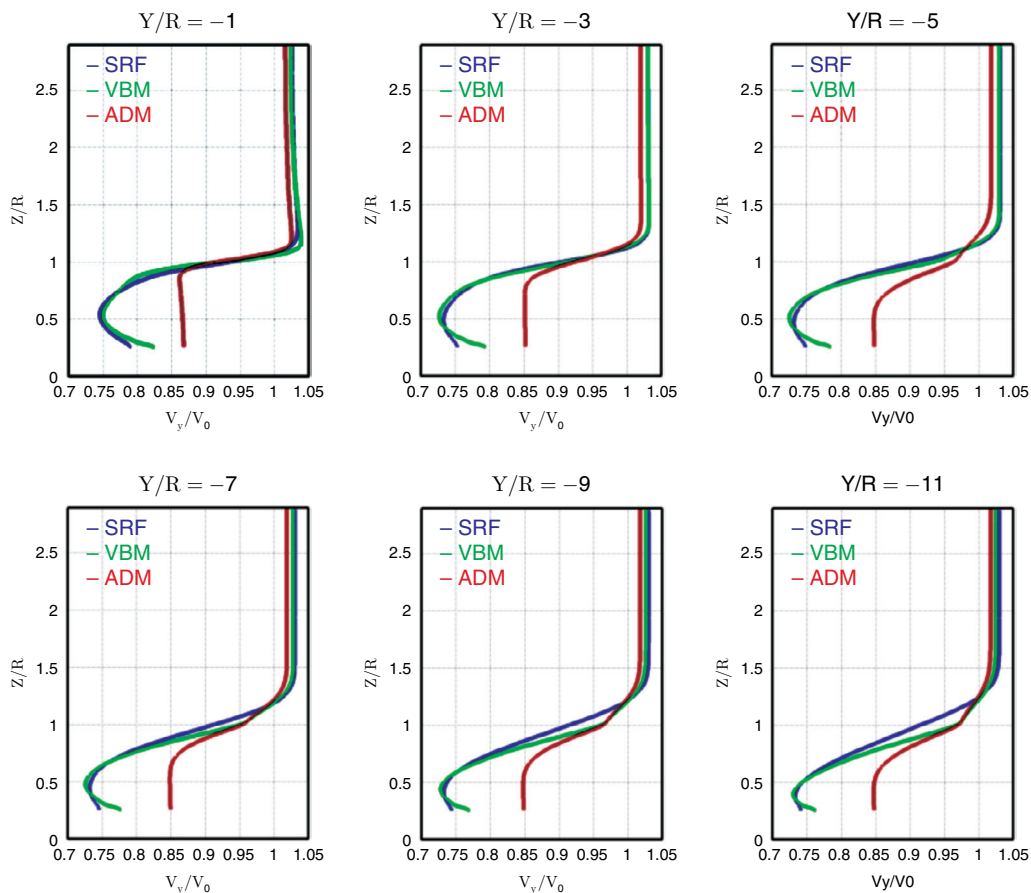
Figure 11. Velocity contours in the turbulent wake simulated via (a) the SRF, (b) the BEM (VBM) and (c) the ADM.

a helical vortex, a result of averaging the blade forces over the rotor. Despite these two differences, the velocity profiles along the channel, shown in figure 12, from the BEM and SRF models are very similar to each other, particularly after a small distance downstream of the blade. Only at $\frac{y}{r} < 1$, there are noticeable differences in the velocity profiles of BEM and SRF.

The flow field simulated using the ADM is presented in figure 11 (c). As can be inferred from the result, a gradual uniform decrease in velocity occurs across the disk, but neither the details of the flow behind the rotor plane nor the tip vortex are captured by this model. The velocity deficit by the ADM in the near wake region is significantly different from the corresponding velocity deficits from the SRF and BEM. A strongly skewed shape, with an almost linear shear section is observed in the near-wake region. After about 3 radii downstream of the device, however, the skewed shape of the simulated velocity profile from the ADM evolve into a smoother shape, closer to the shape of the corresponding velocity profiles modeled with the SRF and the BEM.

Figure 12 shows the detailed comparison of the velocity profiles computed by each model on $Y - Z$ planes at different distances downstream indicated on figures 11 (a) – 11 (c). Overall, the simulated velocity profiles from SRF (in blue) and BEM (in green) show good agreement. The main deviation between them occurs close to the blade root due to flow separation. Since BEM averages the blade forces and does not capture flow separation accurately, it underestimates the velocity deficit in this section of the blade span. Moving further downstream, disagreement of the modeled velocity profiles via SRF and BEM start to become significant at the region close to the blade tip. The lack of flow details at the blade tip in the BEM simulations causes errors in this region. Despite these small differences between the modeled velocity profiles in the wake of the SRF and the BEM simulations, the BEM accurately predicts the far wake behind the turbine, considering the degree of

198   Hierarchical Methodology for the Numerical Simulation of the Flow Field around and
            in the Wake of Horizontal Axis Wind Turbines: Rotating Reference Frame,
            Blade Element Method and Actuator Disk Model

Figure 12. Superimposed velocity profiles simulated with SRF, BEM and ADM models on yz planes

simplification and reduction of computational time and resources. The ADM drastically overestimates the velocity recovery in the near wake, compared to SRF and BEM, but the shape of the velocity profile further downstream becomes more realistic and can serve to study the interactions of turbines at large separation and in topography for wind-farm-scale optimization.

Sørensen et al. [9] provided support for the use of blade-resolved CFD simulations instead of the Blade Element Model, highlighting that they do not rely on empirical input. However, the pros and cons of BEM and ADM simulations versus full-blade geometry computations and its range of applicability in wind turbine studies have not been thoroughly studied. Table 5 provides a quantitative comparison between the required number of mesh elements, number of iterations, computational time (using an 8-core Intel Xeon shared memory workstation) and extracted power for the NREL Phase VI turbine with each model in the proposed methodology presented here. The resulting relative error between turbine power computed from the BEM and SRF is 0.37%. The trade-off presented by BEM lies in the reduction of computational expense and the accuracy of the wake features. The ADM results clearly show consistency with the input of integral performance

Table 5: Comparison between SRF, BEM and ADM results and computational requirements in the simulation of the flow field around a NREL Phase VI HAWT rotor

	SRF	BEM	ADM
Mesh Element [Mill.]	5.10	1.65	1.65
Number of Iterations	12000	2500	500
Computational Time	3 days	3 hours	1 hour
Power [kW]	5.38	5.40	5.74

metrics of the turbine (it requires the drag and power extracted on the turbine for at least one value of the tip speed ratio as inputs to the model) but only rough agreement in the velocity field. However, its low computational cost makes this model appropriate for quick parametric studies or modeling of large numbers of turbines in complex terrain.

5. CONCLUSIONS

We have studied three different numerical models to simulate the dynamics of the flow around a horizontal axis wind turbine (HAWT): the Single Rotating Reference Frame (RRF or SRF), Blade Element Model (BEM) and Actuator Disk Model (ADM). These three models represent widely different representations of the wind turbine rotor fluid mechanics, with a correspondingly wide range of numerical cost, both in terms of CPU time and RAM requirements and in man-hours required to prepare the simulations and postprocess the results. A factor of 10-100 reduction was found between the most detailed simulation, blade-resolving SRF, and the intermediate physics of the BEM. A further factor of 5–10 in computational savings was observed when ADM was used, although with the need of performance as an input and a significant compromise in the accuracy of the wake momentum deficit.

The SRF model is a numerical scheme that accurately simulates the flow field around and in the wake of a wind turbine. It renders the unsteady flow into a steady problem, at the expense of requiring an axisymmetric computational domain. The results presented show that SRF captured the details of the turbulent flow at the root and tip of wind turbine blades by modeling the vortices at the tip and in the near wake region by capturing the detail of the inhomogeneous flow right after the blade passage.

Based on Blade Element Theory, BEM models the time-averaged aerodynamic effects of the rotating blades without the need for creating and meshing their actual geometry. The velocity deficit in the far wake region predicted by BEM in this simulation is in very good agreement with the results from SRF, despite the much higher fidelity to the physics of the latter. This capability, coupled with the significant reduction in computational cost and pre/post processing time shows the promise of BEM in the study of the wake interaction between multiple turbines in a farm of devices, where spacing places them in the far, axisymmetric wake.

We used the ADM, an implementation of the Actuator Disk Theory, as the simplest numerical model that can reproduce the wake of a HAWT. With the efficiency of the turbine as an input, this model produced an approximation to the flow field in the wake of the NREL Phase VI turbine that showed some potential for modeling large turbine farms, although the velocity deficit in the wake needed to be corrected.

We have presented a detailed comparison between three numerical models applied to the flow field of the NREL Phase VI HAWT. The results were carefully validated against experiments and previous simulations in the literature. This work presents clear selection guidelines for numerical implementation of HAWTs in different engineering frameworks (blade design, array optimization, topographic siting, etc.) by presenting a detailed qualitative and quantitative comparison between three numerical models and highlighting their capabilities, and limitations. In conclusion, the SRF model is best suited to simulate the detailed physics of the flow field in the near wake regions of a single HAWT for blade design and optimization. BEM and ADM are adequate to model device arrangements were turbines interact with the far wake. While ADM has a low computational cost and can be combined with complex terrain and large farm length scales (several sq. km.) it requires calibration to accurately represent the momentum deficit and velocity profile development in the wake.

REFERENCES

[1]   Vermeer L-J, Sørensen J-N, and Crespo A. Wind turbine wake aerodynamics. *Progress in aerospace sciences*, 39 (6-7): 467–510, 2003. 27

[2]   Thor S-E and Weis-Taylor P. Long-term research and development needs for wind energy from time frame 2000-2020. *Wind Energy*, 5 (1): 73–5, 2002.

[3]   Vermeer L-J. A review of wind turbine wake research at TUDelft. In *A collection of the* 2001 *ASME Wind Energy Symposium Technical Papers*, *New York*, 2001. p.103–113.

[4]   Hand M-M, Simms D-A, Fingersh L-J, Jager D-W, Cotrell J-R, Schreck S, and Larwood S-M. Unsteady aerodynamics experiment phase 6: Wind tunnel test configurations and available data campaigns. Technical report, National Renewable Energy Laboratory (NREL), 2001.

200   Hierarchical Methodology for the Numerical Simulation of the Flow Field around and
in the Wake of Horizontal Axis Wind Turbines: Rotating Reference Frame,
Blade Element Method and Actuator Disk Model

[5]   Snel H, Schepers J-G, and Montgomerie B. The MEXICO project (model experiments in controlled conditions): The database and first results of data processing and interpetation. *Journal of Physics: Conference Series*, 75 (012014): 1–11, 2007.

[6]   Sørensen N-N and Michelsen J-A. Aerodynamic predictions for the unsteady aerodynamics experiment phase-ii rotor at the national renewable energy laboratory. A*IAA Paper* 2000–0037, 2000.

[7]   Duque E-P-N, Johnson W, van Dam C-P, Cortes R, and Yee K. Numerical predictions of wind turbine power and aerodynamic loads for the NREL phase II combined experiment rotor. *AIAA Paper* 2000–0038, 2000.

[8]   Michelsen J-A and Sørensen N-N. Current developments in Navier- Stokes modelling of wind turbine rotor flow. *In Proceedings of the* 2001 *European Wind Energy Conference and Exhibition*, *WIP-Renewable Energies, Munchen*. P.367–72, 2001.

[9]   Sørensen N-N, Michelsen J-A, and Schreck S. Navier Stokes predictions of the NREL Phase VI Rotor in the NASA Ames 80 ft * 120 ft wind tunnel. *Wind Energy*, 5:151, 2002.

[10]   Le Pape A and Lecanu J. 3D Navier-Stokes computations of a stallregulated wind turbine. *Wind Energy*, 7:309–324, 2004.

[11]   Carcangiu C-E. *CFD-RANS Study of Horizontal Axis Wind Turbines*. PhD thesis, Universita degli Studi di Cagliari, 2008.

[12]   Sørensen J.N. *Comprehensive Renewable Energy* (*Wind Energy*, *Vol*.2). Elsevier Ltd., 2012.

[13]   Simms D, Schreck S, Hand M, and Fingersh L-J. NREL unsteady aerodynamics experiment in the NASA-AMES wind tunnel: A comparison of predictions to measurements. Technical report, National Renewable Energy Laboratory (NREL), 2001.

[14]   Glauert H. *Aerodynamic theory,* chapter Division L, vol. 4. Berlin, germany, pages 169–360. Julius Springer, 1935.

[15]   Laith Z and Rajagopalan R. Navier-Stokes calculations of rotor-airframe interaction in forward flight. *Journal of the American Helicopter Society*, 40 (2): 57, 1995.

[16]   Crespo A, Hernandez J, and Frandsen S. Survey of modelling methods for wind turbine wakes and wind farms. *Wind Energy*, 2 (1): 1–24, 1999.

[17]   Makridis M and Chick J. CFD modeling of the wake interactions of two wind turbines on a Gaussian hill. In *WEACWE* 5, *Florence*, *Italy*, 2009.

[18]   Lanzafame R and Messina M. Fluid dynamics wind turbine design: Critical analysis, optimization and application of bem theory. *Renewable Energy*, 32:2291–2305, 2007.

[19]   Lanzafame R and Messina M. Horizontal axis wind turbine working at maximum power coefficient continuously. *Renewable Energy*, 35:301–306, 2010.

[20]   Ruith M. Unstructured, Multiplex rotor Source Model With Thrust and Moment Trimming - FLUENT's VBM Model. In *AIAA Applied Aerodynamics Conference*, 2005.

[21]   Pinheiro Vaz J-R, Pinho J-T, and Mesquita A-L-A. An extension of bem method applied to horizontal-axis wind turbine design. *Renewable Energy*, 36:1734–1740, 2011.

[22]   Froude R-E. On the part played in propulsion by difference of fluid pressure. *Trans Inst Naval Arch*, 30:390–405, 1889.

[23]   van Kuik G-A-M. *On the limitations of froude's actuator disc concept*. PhD thesis, Eindoven University of Technology, February 1991.

[24]   Mikkelsen R. *Actuator disc methods applied to wind turbines*. PhD thesis, Technical University of Denmark, 2003.

[25]   Crastoa G, Gravdahla A-R, Castellanib F, and Piccionib E. Wake modeling with the actuator disc concept. *Energy Procedia*, 24:385–392, 2012.

[26]   Castellani F and Vignaroli A. An application of the actuator disc model for wind turbine wakes calculations. *Applied Energy*, 101:432–440, 2013.

[27]   Bertagnolio F, Sørensen N-N, and Johansen J. Profile catalogue for airfoil sections based on 3D computations. Technical report, Riso National Laboratory, 2006.

[28] Tangler J-L. The nebulous art of using wind-tunnel airfoil data for predicting rotor performance: Preprint. In *The* 21*st ASME Wind Energy Conference, Reno, Nevada, January* 14–17, 2012.

[29] Warsi Z-U-A. Fluid Dynamics, Theoretical and Computational Approaches. CRC Press, 1993.

[30] Burton T., Sharpe D., Jenjins N. and Bossanyi E. *Wind energy handbook*. Wiley, 2000.

[31] Javaherchi T. Numerical modeling of tidal turbines: Methodology development and potential physical environmental effects. Master's thesis, University of Washington, 2010.

[32] Twidell J and Weir T. *Renewable Energy Resources* (2*nd edition*). Taylor & Francis, 2006.

[33] Spalart P-R and Allmaras S-R. A one equation turbulence model for aerodynamic flows. *In AIAA* 92-0439, *AIAA* 30*th Aerospace Sciences Meeting and Exhibit*, Reno, NV, January 1992.

[34] Potsdam M and Pullian T. Turbulence modeling treatment for rotorcraft wakes. In *AHS Specialist's Conference on Aeromechanics,* Jan. 23–25 2008.

[35] Wilcox D-C. *Turbulence Modeling for CFD, 3rd edition*. DCW Industries, Inc., La Canada CA, 2006.

[36] Menter F-R. Two-equation eddy-viscosity turbulence models for engineering applications. *AIAA Journal*, 32 (8): 1598–1605, 1994.

[37] Somers D. Design and experimental results for the S809 airfoil. Technical report, National Renewable Energy Laboratory, Colorado, USA, 1997.

[38] Pope S-B. *Turbulent Flows*. Cambridge University Press, 2006.

[39] Nee V-W and Kovasznay L-S-G. Simple phenomenological theory of turbulent shear flow. *Physics of Fluids*, 12: 473–484, 1969.